catalysts

MDPI

Article

Synthesis and Characterization of Novel Phyto-Mediated Catalyst, and Its Application for a Selective Oxidation of (VAL) into Vanillin under Visible Light

Afnan Al-Hunaiti [1,*], Qassem Mohaidat [2], Ibrahim Bsoul [3], Sami Mahmood [4,5], Deeb Taher [1] and Tareq Hussein [4,6,*]

1 Department of Chemistry, The University of Jordan, Amman 11942, Jordan; d.taher@ju.edu.jo
2 Department of Physics, Yarmouk University, Irbid 21163, Jordan; q.muhaidat@yu.edu.jo
3 Department of Physics, Al al-Bayt University, Mafraq 13040, Jordan; ibrahimbsoul@yahoo.com
4 Department of Physics, The University of Jordan, Amman 11942, Jordan; s.mahmood@ju.edu.jo
5 Department of Physics and Astronomy, Michigan State University, East Lansing, MI 48824, USA
6 Institute for Atmospheric and Earth System Research (INAR), University of Helsinki, PL 64, UHEL, FI-00014 Helsinki, Finland
* Correspondence: a.alhunaiti@ju.edu.jo (A.A.-H.); tareq.hussein@helsinki.fi (T.H.)

Received: 4 July 2020; Accepted: 21 July 2020; Published: 24 July 2020

Abstract: Here, we report an efficient and highly selective oxidation of lignin model substrate using phyto-mediated $ZnFe_2O_4$ nanoparticle using *Boswellia carterii* extract. The nanocatalyst with an average size of 8 nm showed excellent photocatalytic activity of the synthesized carbonyl containing products under visible light irradiation. The catalytic activity and selectivity towards oxidation of vanillyl alcohol to vanillin with selectivity up to 99% at conversion over 98% and turn-over frequency values up to 1600 h^{-1} were obtained in the presence of H_2O_2 and base. The cubic spinel nano-$ZnFe_2O_4$ catalyst was characterized by powder-XRD, FESEM, HR-TEM and Mössbauer analysis. The demonstrated catalyst was robust and stable under the reaction conditions. Furthermore, it was easy to be separated from the reaction mixture and be reused for subsequent reactions up to 5 times without significant reactivity or selectivity loss.

Keywords: lignin; hydrogen peroxide; vanillyl alcohol; oxidation; nanoparticle; green catalyst; selective; visible light

1. Introduction

The upsurge need of alternative sources for fine chemicals take the burden off the dependency on depleted traditional non-renewed sources and might have environmental benefits [1–3]. Valorization of renewable lignocellulosic biomass has been considered as a critical step toward sustainability. Lignin is an aromatic amorphous polymeric material that encompasses important classes of aromatic compounds [4–6]. The valorization of lignin compounds by converting lignin into valuable fine chemicals and fuels has become an appealing approach. Previously, several strategies to produce lignin derivatives, including pyrolysis, hydro processing and oxidation were reported [7–11].

In comparison to thermal and hydro processing strategies, which require high energy input, oxidation strategies are gaining intensive attentions because they can be implemented under mild and environmentally friendly conditions [11–25]. The oxidative depolymerization has been viewed as a promising method for the conversion of lignin to small phenolic compounds such as vanillin, syringaldehyde and p-hydroxybenzaldehyde [11–17]. Many homogeneous and heterogeneous catalysts

have been used for the oxidation of both lignin and lignin model compounds. The studies were performed in ionic liquids, acidic, alkaline or organic media. For example, vanillin was produced from lignin in concentrated alkaline medium, under oxygen pressure, in the presence of a transition metal [11]. Vanillyl alcohol (VAL) is considered a lignin model substrate that is particularly interesting because it can be converted selectively into vanillin (4-hydroxy-3-methoxybenzaldehyde), which is one of the few value-added chemicals commercially produced from lignin [12–18]. Vanillin along with its derivatives have many applications in food, perfume and pharmaceutical industries [12–19].

The selective oxidation is one of the major transformations in organic chemistry. Replacement of stoichiometric poisonous oxidants with catalytic systems employing air (i.e., oxygen) as a terminal oxidant is an important goal in green chemistry [20]. Over the past few years, transition bimetallic and trimetallic nano-particles (NPs) have been given increasing attention because they show higher catalytic activities compared with monometallic NPs in many applications and reactions [21]. For example, $ZnFe_2O_4$ received great interest due to its wide applications in nanomaterial, adsorption, photocatalysis and solar cells [22–28]. For instance, photochemical degradation of organic contaminants using H_2O_2/UV has been widely studied, where the photodegradation efficiency depends on the decomposition rate of H_2O_2 [29]. Many perovskite or spinel type complex oxides have been found to have visible-light-driven photoactivity. The spinel $ZnFe_2O_4$ with a relatively narrow band gap of about 1.9 eV was used in the solar energy, photocatalysis and photochemical hydrogen production from water due to its visible-light response, good photochemical stability and low cost [30]. As $ZnFe_2O_4$ particles are magnetic semiconductor materials [19,20], $ZnFe_2O_4$ based catalysts can be magnetically separable in a suspension system by virtue of their own magnetic properties without tedious work-up after the reaction. Therefore, the controlled synthesis of $ZnFe_2O_4$ nanomaterials with a desirable morphology, structures and properties is still challenging. A phyto mediated synthesis of nanoparticles have gained great attention lately as it opened new paths in different fields, and implementation of its usage as a reducing agent in the NPs preparation has been a very useful clean, ecofriendly and cost effective preparation technique. In very close correlation with their content in bioactive molecules, plant extracts have been successfully used to generate transition metal nanoparticles and iron-based magnetic nanoparticles among these metals [31–34].

In the present investigation, $ZnFe_2O_4$ nanoparticles were synthesized by treating with a mixture of metal acetate and iron chloride with the aqueous extract of *Boswellia carterii* resin. This extract is dried gum resin of *Boswellia carterii*, which is one of 43 species in the genus *Boswellia* of the family Burseraceae. Previous studies have shown that the boswellic acids and various other acids are isolated from frankincense [35,36]. Here, we use the extract as a reducing agent to produce bimetallic $ZnFe_2O_4$ nanoparticles. The NPs were also used under visible light and H_2O_2 for selective oxidation of (VAL) into vanillin under green environmentally friendly condition. Various analytic methods for characterization of the synthesized $ZnFe_2O_4$ bimetallic nanoparticles (XRD, TGA, IR, SEM and HR-TEM) were applied for the evaluation and the characterization of the phytosynthesized nanocatalyst.

2. Results and Discussion

Different studies stressed out that plant metabolites like polyphenols are natural reducing agents and a capping agent used for metallic nanoparticles stabilization [37]. This effect was most emphasized when different solvent extraction was used the quantities of polyphenols had a significant variation. Hence the effectiveness in the formation and stabilization of nanoparticles also varied. As a first step a preliminary phytochemical screening of the analytic protocol was developed for *Boswellia carterii* resin. The previous studies in phytochemical analysis revealed more abundant glycosides, saponins and tannins, which match with previous studies regarding this plant [37]. Aqueous extract contains saponins and tannins. The obtained GC-MS results are consistent with the literature data regarding these plant extracts [37]. Upon the addition of the reducing agent (aqueous extract) a color change can be rapidly observed. In the present study, we did speculate that various compounds such as boswellic

acid might be able to generate and stabilize the $ZnFe_2O_4$ nanoparticles as it was found at a large extent in the extract and can act as a reducing and capping agent in the process.

2.1. Structural Analysis

In the spinel structure with molecular formula $MeFe_2O_4$ (Me is a divalent ion), the metal ions are distributed such that one ion per molecule occupies the tetrahedral (A) site, and two occupy the octahedral (B) site. The A-B antiferromagnetic super exchange interactions between magnetic ions at A and B sites is much stronger than the A-A and B-B interactions, resulting in two magnetic sublattices, namely, the spin-down A and spin-up B sublattices [38,39]. Accordingly, the spinel is generally a ferrimagnetic material with magnetization determined by the net magnetization of the two sublattices ($M_B - M_A$), exhibiting ferromagnetic-like behavior. In the normal spinel structure, the divalent Me^{2+} ion occupies tetrahedral spin-down sites, whereas the two trivalent Fe^{3+} ions occupy the octahedral spin-up sites. In the inverse spinel structure, however, the Me^{2+} ion occupies the octahedral site, and the Fe^{3+} ions are distributed equally between tetrahedral and octahedral sites. In this case, the magnetic moments of Fe^{3+} ions at spin-up (B) and spin-down (A) sites cancel out, and the net magnetic moment per molecule is completely determined by the magnetic moment of the Me^{2+} ion. Normally, the Zn^{2+} ion demonstrates preference for tetrahedral sites [38], and therefore, the Zn-ferrite is recognized as a normal spinel. In this case, there are no magnetic ions at the A sites to align the magnetic moments in the B sublattice, and the compound behaves like a paramagnetic material [38]. Consequently, the $ZnFe_2O_4$ normal spinel is expected to exhibit almost a linear increase of the magnetization with the increase of the applied magnetic field intensity (H) in the range of this study. However, if there is some degree of inversion in the spinel structure (where a fraction of the Zn^{2+} ions occupies the octahedral sites and an equal fraction of Fe^{3+} ions is pushed into the tetrahedral sites), then the super exchange interactions align the A and B sublattices, and the magnetization may show a saturation behavior with the increase of H.

The X-ray diffraction pattern of the zinc iron ferrite (Figure 1) clearly revealed a major cubic (fcc) spinel phase, whose reflections are labeled by their respective Miller indices (hkl). In addition, weak peaks corresponding to an impurity unidentified phase are observed. The relation between the d-spacing between atomic planes in the crystal lattice and the angular position (θ) of the diffraction peak is described by Bragg's law:

$$2d \sin\theta = \lambda \quad (1)$$

where λ is the wavelength of the Cu-K_α radiation (=1.5406 Å). For cubic crystals, the relation between the d-spacing and the lattice constant (a) is given by the relation:

$$d = \frac{a}{\sqrt{h^2 + k^2 + l^2}} \quad (2)$$

Accordingly, a plot of $(\lambda/2)\sqrt{h^2 + k^2 + l^2}$ vs. $\sin\theta$ should give a straight line passing through the origin, and having a slope equal to the lattice constant (a). Figure 2 shows a perfect straight line indicating the reliability of indexing the reflections (Figure 1) in terms of a cubic spinel structure. The lattice constant ($a = 8.365 \pm 0.010$ Å) was obtained from the slope of the linear fit to the experimental data. This value is consistent with the reported values of 8.34–8.41 Å [40].

The structure and morphology of the synthesized nanoparticles are shown in the FESEM and HRTEM images (Figures 3 and 4). The particle size distribution (Figure 3b) revealed an average particle size of 8 Å, whereas HRTEMs particle sizes were between 7.5 and 18 nm (Figure 4). The FT-IR spectrum of the nano $ZnFe_2O_4$ exhibited a broad band at 3421 cm^{-1} associated with the stretching mode of H_2O molecules, indicating the presence of OH groups on the surface of nanoparticles. The band at 1637 cm^{-1} corresponded to the bending mode of H_2O molecules. The absorption bands in the range of 1000–400 cm^{-1} were assigned to metal-oxygen stretching vibrations of the ferrite spinel structure. A strong band at 548 cm^{-1} was related to the Fe-O stretching vibration at the tetrahedral site.

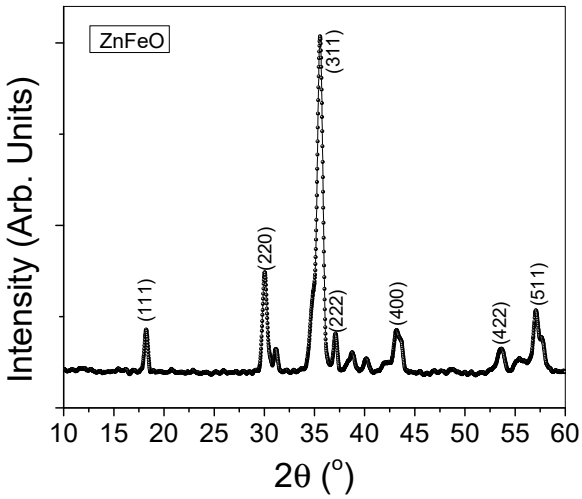

Figure 1. X-ray diffraction pattern of Zn-ferrite.

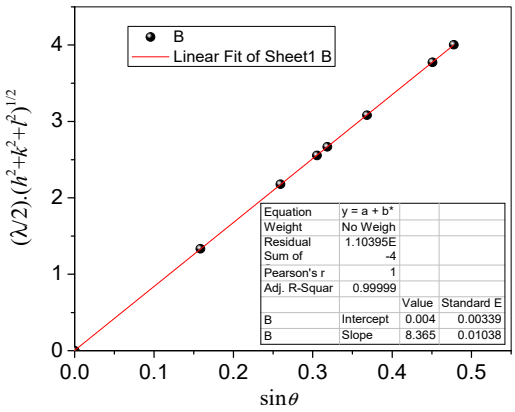

Figure 2. A plot showing the relation between the Miller indices and the angular positions of the diffraction peaks for the spinel phase.

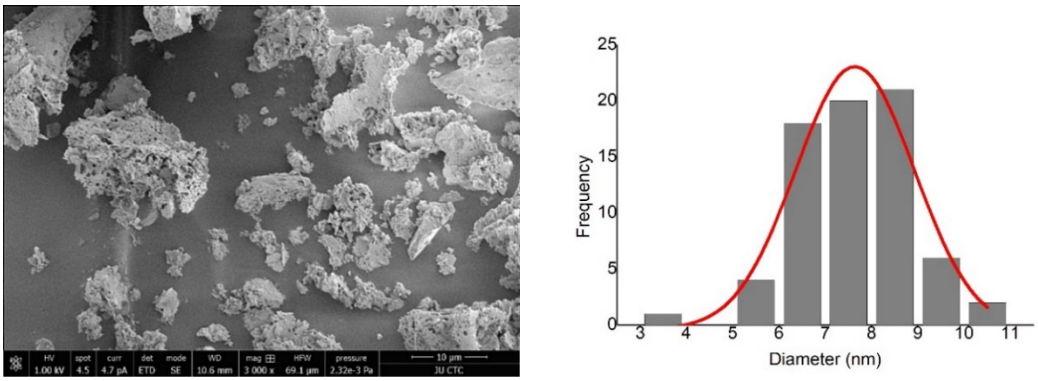

Figure 3. (**a**) FESEM images of the $ZnFe_2O_4$-NP and (**b**) particle size distribution with a Gaussian fit $y = y_0 + \frac{A}{w\sqrt{\frac{\pi}{2}}}e^{-2\left(\frac{x-x_c}{w}\right)^2}$ with $\frac{Chi^2}{DoF} = 7.51248$ and $R^2 = 0.94765$, where $y_0 = -0.37631 \pm 2.24235$, $x_c = 7.64135 \pm 0.1408$, $w = 2.56395 \pm 0.43159$, and $A = 75.2894 \pm 16.57784$.

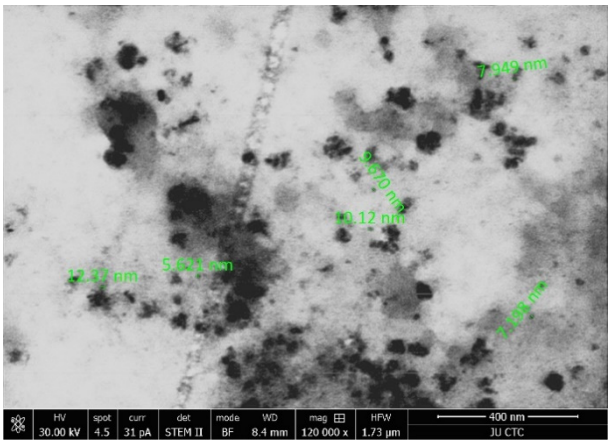

Figure 4. HRTEM images of the nanoparticles.

2.2. Magnetization

The initial magnetization curve and the magnetic hysteresis loop of the ferrite are shown in Figure 5. As clearly seen in Figure 5a, the magnetization increased sharply with the increase of field intensity (H) in the low field range, and then tended to saturate at high fields. This behavior is characteristic of a soft magnetic material. The narrow hysteresis loop in Figure 5b revealed a low coercivity (H_c), confirming the soft magnetic character of the sample. The ferromagnetic behavior with an approach to saturation in the high field range indicates some degree of inversion in the $ZnFe_2O_4$ spinel. The saturation magnetization (M_s) was obtained from a plot of M vs. $1/H$ in the high field range by extrapolating to $1/H = 0$. Following the analysis in Mahmood's study [41], the slope of the straight line was used to determine the lower limit (D_s) of the particle diameter in the sample. Additionally, the upper limit of the particle diameter (D_l) was determined from the initial magnetic susceptibility using the analysis provided in the same reference. The evaluated quantities in Table 1 indicate that the magnetic particle diameter in the sample ranges between 7.4 and 13.5 nm. This range of particle size is consistent with the typical range of diameters for superparamagnetic particles in spinel ferrites [40,42], and with the results of FESEM and HRTEM analyses.

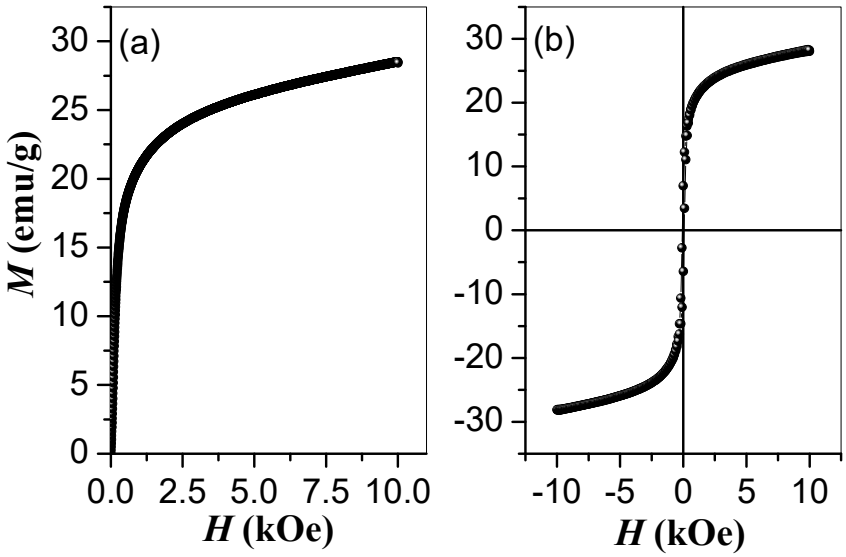

Figure 5. Initial magnetization curve (**a**), and hysteresis loop (**b**) of the $ZnFe_2O_4$ spinel ferrites.

Table 1. Magnetic parameters and range of particle diameters for the $ZnFe_2O_4$ sample.

M_s (emu/g)	H_c (Oe)	D_s (nm)	D_l (nm)
32.3	65	7.4	13.5

The Mössbauer spectrum of the Zn-ferrite (Figure 6) shows a paramagnetic doublet with quadrupole splitting of 0.40 mm/s and a chemical isomer shift of 0.24 mm/s. The seemingly contradictory results of the magnetic and Mössbauer measurements could be explained by the different time scales of the two experimental techniques [43]. The fast relaxations of the magnetic moments of the superparamagnetic particles at room temperature appear to Mössbauer spectroscopy as if the particles have no net magnetic moment, resulting in a paramagnetic signal. However, in the magnetic measurements, the applied field aligns the magnetic moments, resulting in a ferromagnetic-like behavior. Similar ferromagnetic behavior in the magnetization measurements and paramagnetic behavior in Mössbauer spectroscopy was recently reported for ferrites [40,44].

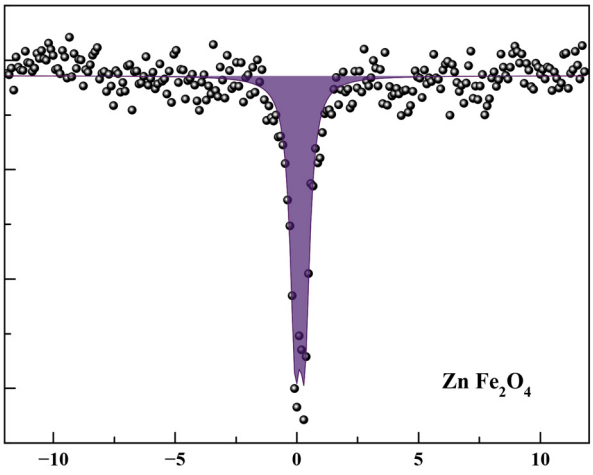

Figure 6. Mössbauer spectrum of Zn-ferrite.

2.3. Oxidation of Vanillyl Alcohol

We investigated the reactivity of $ZnFe_2O_4$-NP and its loading towards the oxidation of lignin substrate model VAL alcohol. We also studied the effect of light intensity, base type and oxidant amount. Initially, we tested the reactivity of $ZnFe_2O_4$-NP (2 mg) as a catalyst (Scheme 1) and H_2O_2 as an oxidant in MeCN. This gave poor conversion with vanillin as a main product (12%, 20 h).

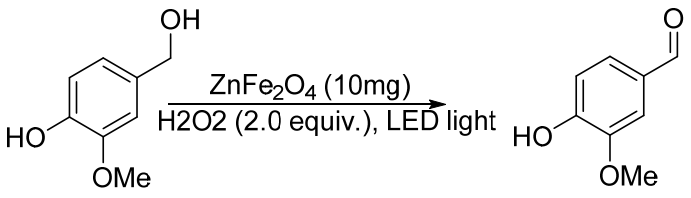

Scheme 1. Selective oxidation of vanillin with $ZnFe_2O_4$ nanoparticle catalysts.

After optimization, the catalyst showed a high reactivity with high selectivity toward vanillin. Interestingly, until now no studies have used visible light induced photocatalysis of $ZnFe_2O_4$ in lignin substrate model oxidation. Previously the VAL oxidation was studied as a lignin model substrate using heterogeneous catalysis with a series of Pt and Pd immobilized on modified carbon carriers (sibunit, SKT-6 and SKT-4) on various metal oxides such as TiO_2, SiO_2 and MgO or metal organic framework

(Table 2). Most of these catalysts converted VAL into vanillin with 24–69.6% Yield under basic or acidic solutions, and through a simple regeneration technique the catalysts were reused for several times.

Table 2. Oxidation of VAL using a heterogeneous catalyst.

Entry	Catalyst	Experimental Conditions	Products	Yield (%)	References
1	Co_3O_4	413 K 0.689–4 MPa H_2O 7 h	Vanillic acid	69.6	[45]
			Vanillin and others	9.4	
2	Mn-Co (mixed oxide)	433 K 2.1 MPa MeCN 4 h	Vanillin	60	[18]
			Vanillic acid and others	24	
3	Mn_2O_3	433 K 2.1 MPa MeCN 2 h	Vanillin	54	[18]
			Vanillic acid and others	18.4	
4	1% Pd Sibunit	353 K NaOH/H_2O 1 h	Vanillin	34.8	[46]
5	2.3% Pt MgO	353 K NaOH/H_2O 1 h	Vanillin	48	[46]
6	$CoTiO_4$ H_2O_2	298 K MeOH CH_3COOH 6 h	Vanillic acid	31	[47]
			Vanillin	68	
7	$ZnFe_2O_4$ Visible light H_2O_2	298 K TBAOH MeCN 2 h	Vanillin	99	This work

2.3.1. The Effect of the Oxidant (H_2O_2) Amount

Increasing the oxidant amount as 2.5 equivalent of H_2O_2 in isopropyl alcohol as a solvent, the yield was increased to be 83% of corresponding aldehyde (Figure 7). In the absence of a catalyst and using hydrogen peroxide, 25% yield was obtained with a lack of selectivity. As blank experiments for catalysis, ZnO and Fe_2O_3 oxides gave moderate yields.

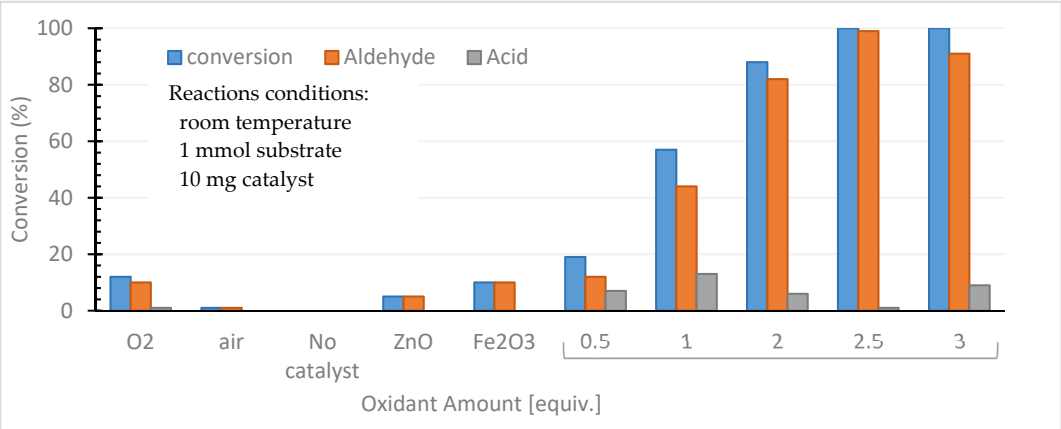

Figure 7. Reactivity of $ZnFe_2O_4$-NP in the presence of the different oxidant (H_2O_2) amounts and compared to blank experiments (ZnO and Fe_2O_3) and no oxidant.

2.3.2. The Effect of Light Intensity and Type on the Photocatalytic Oxidation of VAL Alcohol

We tested the photocatalytic oxidation of VAL alcohol by using a UV-light source and three visible light intensities (LED visible light). The used LED light was identical in the type of light (IKEA, RYET/TRÅDFRI white light) with the difference in the luminous and power being: 3 watt (200 lm), 5 watt (400 lm) and 7 watt (600 lm). As for the UV-light source, it was Philips TUV 6W G6 T5 UVC UltraViolet Sterilizer Lamp Tube UV.

The results were compared to the reaction in the dark (Figure 8). Upon UV light irradiation, the alcohol conversion was excellent, but the reaction was not selective with respect to aldehyde formation; the selectivity was 67% toward vanillin. Using an LED visible light source, the photocatalytic oxidation was enhanced by increasing the light intensity. For instance, increasing the visible light intensity enhanced the reaction to produce 74% of vanillin, which was more than four times that was obtained in the absence of light. Visible light illumination of the NP catalyst clearly enhanced the oxidation process.

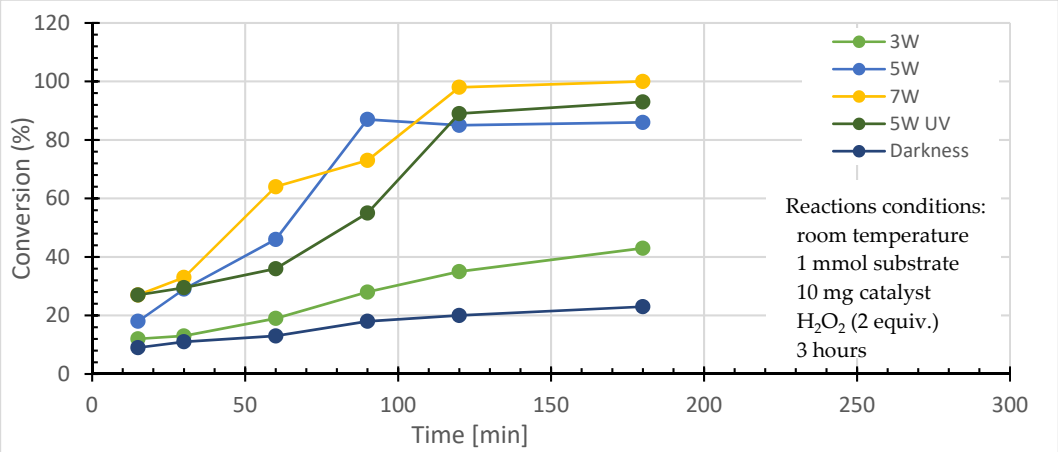

Figure 8. Optimization with respect to light intensity.

The effect of light type and intensity is expected because the photons excite valence electrons and bring them to the conduction band; therefore, increasing the light intensity enhances the catalytic reactivity of the $ZnFe_2O_4$ nanoparticles [48–55]. Not only does the intensity of the radiation influence the oxidation rate of photocatalytic activity, but also the wavelength of irradiated light is one of the main factors of the system's efficiency [56]. In our case, the reaction took place in acetonitrile solvent (CH_3CN); and hence, the interaction of acetonitrile with the surface was previously demonstrated by its quenching of luminescence from band gap energy levels via nitrogen [18]. The formation of active oxygen species, particularly superoxide radicals, was proposed to be a key channel leading to aldehyde formation. Nevertheless, the possibility of the acetonitrile playing an active role in the reaction mechanism cannot be ruled out as acetonitrile has been previously reported to promote the formation of active radical species [51–55]. Furthermore, oxygen peroxide species were found to be responsible for alcohol oxidation, for example, $ZnFe_2O_4$ produced 17% of the vanillin in the dark as a result of the high activity of catalyst particles.

The possibility of dry acetonitrile playing an active role in the reaction mechanism cannot be ruled out as acetonitrile has been previously reported to promote the formation of active radical species [48–50]. Moreover, photogenerated electrons in the conduction band reduced the dissolved oxygen species and peroxide species; resulting in superoxide ions. Such superoxide ions have an oxidation potential to generate (OH) radicals from H_2O and hydroxyl ions. The reactive OH radicals can oxidize alcohol into aldehyde. Correspondingly, similar mechanism could explain the increasing conversions with increasing hydroxide ion concentration in the reaction. A further detailed study regarding this catalyst mechanism is ongoing.

2.3.3. Effect of $ZnFe_2O_4$-NPs Loading

When the $ZnFe_2O_4$-NP loading was decreased from 10 to 5 mg (i.e., 0.34–0.08 mmol), the reaction rate was slowed down to be 45% conversion and 99% selectivity to vanillin (Figure 9). When the $ZnFe_2O_4$-NP loading was increased from 10 to 20 mg (i.e., 0.34–0.05 mmol), the reactivity remained the same but the selectivity to aldehyde was reduced significantly. Product formation was not observed in the absence of the catalyst, which were blank experiments (Figure 7).

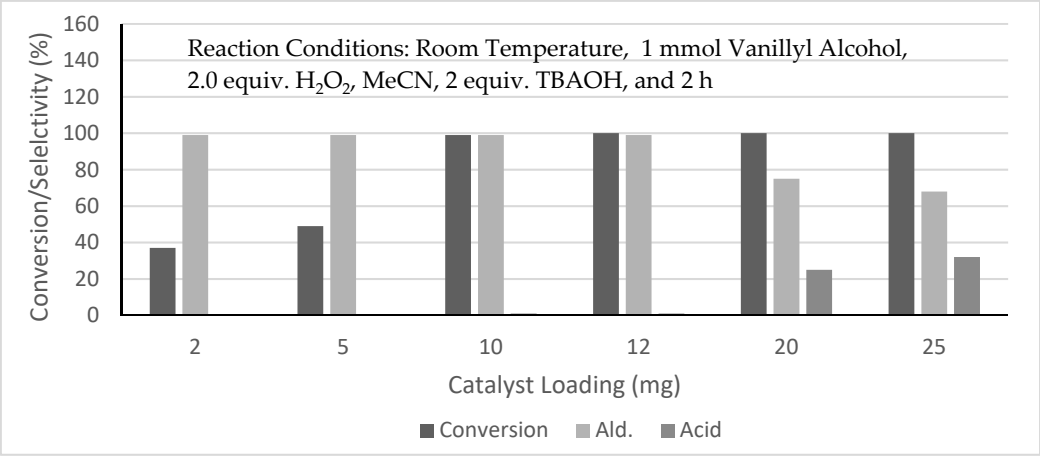

Figure 9. The effect of the $ZnFe_2O_4$-NP catalyst loading in toluene oxidation.

2.3.4. Effect of the Base

Next, according to previous reports the addition of a base is required to oxidize alcohol to aldehyde [12–19]. In a control experiment when the substrate (VAL) was oxidized with no base added to the reaction, only 15% conversion with no selectivity to vanillin was observed. Hence, we decided to study the effect of base by adding 2 equiv. of various bases in a 180 min reaction (Figure 10). The most affected increase of conversion from 35 to 99% was achieved by using tetra butyl ammonium hydroxide (TBAOH) salt as a base with selectivity to vanillin up to 99%, showing that the additional base prevents undesired side reactions. In particular, the reaction reached a high turn-over frequency (TOF) value of 1600 h^{-1} after 60 min with 2 equiv. of TBAOH added. After having the optimization condition in hands we tested these conditions for the oxidation of another lignin substrate models veratryl alcohol and p-anisinic alcohol, and to our delight we obtained the aldehyde product selectively with 89–95% yields (Table 3 entry 2 and 3).

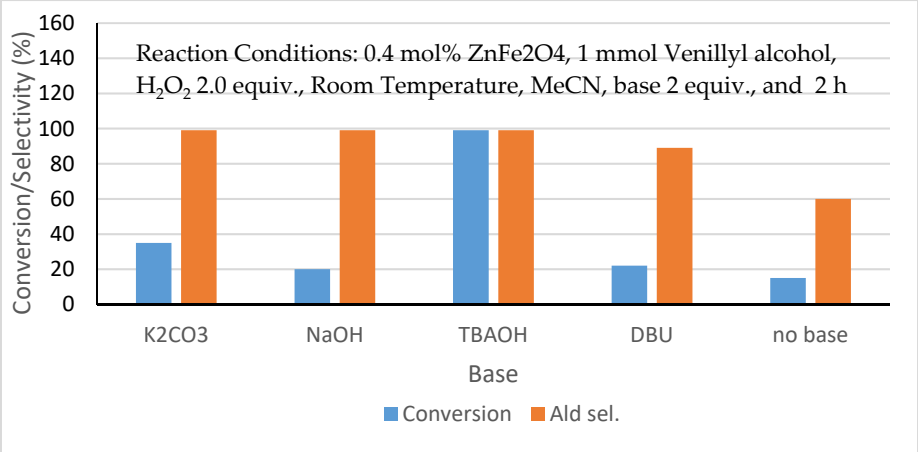

Figure 10. Effect of base type. 0.4 mol% $ZnFe_2O_4$ using different bases. Reaction conditions: 1 mmol vanillyl alcohol, 2.0 equivalent H_2O_2, rt, MeCN, base 2 equiv. and 2 h reaction time.

Table 3. Oxidation of other lignin substrate models.

Entry	Substrate	Yield (Ald. Selectivity) (%) [1]
1	Vanillyl alcohol	99 (99)
2	Veratryl alcohol	95 (99)
3	p-anisinic alcohol	89 (95)

[1] Reaction conditions: 1 mmol alcohol, 2.0 equivalent H_2O_2, rt, MeCN, TBAOH 2 equiv. and 2 h reaction time. Yield was isolated yield.

Previously, it was reported that vanillin undergoes autocatalytic oxidation via radical mechanisms [56], which were suppressed by employing high concentrations of alkali in the production of vanillin by oxidative cleavage of lignin [7,8,57]. Furthermore, deprotonation of the phenolic hydroxyl and delocalization of the negative charge hinders further oxidation of the aldehyde to the acid [57].

2.4. Recyclability

It was evident that this catalyst could be reused two times without activity loss (Figure 11a). After the fifth time, the catalyst weight loss was about 15 wt % and the conversion/selectivity was within 60% and 80%. The drop in the reactivity was possibly due to change in morphology in the nanoparticles and leaching the metals as shown in Figure 11b. Recyclability is an important feature of heterogeneous catalysis [58,59].

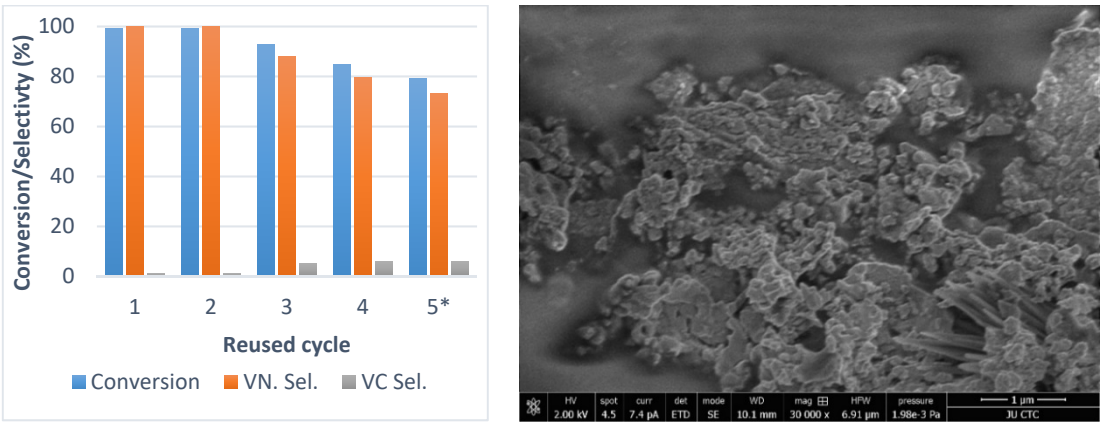

(**a**) (**b**)

Figure 11. (**a**) Recyclability test of the $ZnFe_2O_4$-NP catalyst where VN is vanillin and VC is vanillic acid and (**b**) SEM image of the $ZnFe_2O_4$-NP catalyst after the 5th cycle.

3. Materials and Methods

3.1. Chemicals, Solvents and Starting Materials

Iron (III) chloride anhydrous, zinc acetate and all solvents were purchased from Sigma-Aldrich and used as received except acetonitril (MeCN) was dried under molecular sieves. The structural analysis of MFe_2O_4 nanoferrites were confirmed by powder X-ray diffraction (P-XRD, Cu-K_α radiation, nickel filter, 40 kV, 30 mA and range 4–600, (SHIMADZU XRD-7000, Japan)), scanning electron microscope (SEM (JEOL 6400 and FEI QUANTA 200, Japan)), infrared (RX-FTIR, KBr discs, 4000–300 cm^{-1}, (Perkin Elmer, USA)) and gas chromatography (GC–MS, FID detector, RTx-5ms capillary column (30 m × 0.25 mm), 350 °C, (Saturn 2200, Varian Inc., LabX, Canada)).

Ultra high purity helium (99.999%) was used as a carrier gas at a constant flow rate of 1.0 mL/min. The injection, transfer line and ion source temperatures were 270 °C, 240 °C and 240 °C, respectively. The injected sample volume was 1 mL, with a split ratio of 50:1. The oven temperature was increased from 60 °C to the final temperature of 240 °C at a rate of 3 °C/min.

3.2. Preparation of Plant Extract

The *Boswellia carterii* resin material were washed to remove the adhering particles, and 20 g of plant segments was ground using a mortar and pestle, and the mixture was boiled in a 250 mL Erlenmeyer flask with 200 mL water for 2 h. The aqueous extract was filtered and evaluated for the synthesis of nanoparticles. The unknown compounds were identified by comparing the spectra obtained with mass spectrum libraries (NIST 2011 v.2.3 and Wiley, 9th edition).

3.3. Synthesis of Bimetallic $ZnFe_2O_4$ Nanoparticles and Charaterization

The aqueous extract was treated with a mixture of 1 mM Zn acetate $Zn(CH_3CO_2).H_2O$, and 1 mM iron (III) chloride (1:1 *v*/*v*). The initial synthesis was monitored with a change in color of the reaction mixture into dark brown. The reaction was stirred for 1 hand afterward the pH of the mixture was adjusted to 10–12 using NaOH solution. The product was centrifuged, the solid was isolated, oven dried at 80 °C for 4 h and then washed with water to obtain the neutral solution. The crystalline nature of bimetallic nanoparticles was studied using XRD analysis. The bimetallic nanoparticles were centrifuged, and later adequate amount of sample was coated onto the XRD grid.

3.4. Mössbauer Spectroscopy

Mössbauer samples were prepared as a thin circular layer of the system powder pressed gently between two Teflon disks with a diameter 2 cm, which is small compared with the distance between the source and the sample in order to avoid angular broadening of the spectrum. ^{57}Fe Mössbauer spectra were recorded using a standard constant acceleration Mössbauer spectrometer over 1024 channels with a ^{57}Co/Rh source. The spectra were then calibrated using iron metal spectrum at room temperature and the experimental spectra were fitted using routines based on the least squares analysis.

3.5. Photocatalytic Reaction

The prepared $ZnFe_2O_4$ NPs were used in the oxidation of VAL. A 1 mmol of vanillyl alcohol, (0.0107 mmol, 10 mg) of the magnetic $ZnFe_2O_4$-NP, 2 mmol of TBAOH and H_2O_2 (2 mmol) were added to a round bottom flask under magnetic stirring at room temperature in the dark (Scheme 1). Then the solution was irradiated by a visible light source using a 10 W LED lamp. Before starting the illumination, the reaction mixture was stirred for 30 min in the dark in order to reach the adsorption–desorption equilibrium between the dye and the catalyst. After adding 0.5 mL of 30% H_2O_2 to the above reaction mixture, the lamp was turned on. At a given time interval of irradiation, the catalyst was removed by a magnet, and the samples were taken to the analysis. The samples were analyzed by GC–MS and then the confirmation of the products was done by ^{1}H-NMR and ^{13}C-NMR and compared to commercially available chemicals.

Conversion efficiency of VAL to VN was determined as follows [46,60,61]:

- Conversion (%) (CVN) = (VN/Total VAL) × 100%;
- Selectivity (%) (S) = (An interested product (mol)/Consumed VAL (mol) × 100%;
- Yield (%) (YVN) = conversion × selectivity = (VN produced (mol)/Total VAL (mol)) × 100%.

Turn-over frequencies (TOFs) per surface atom were calculated according to:

$$TOF = \frac{n\ substrate * C}{n\ ZnFe_2O_4 * D\ ZnFe_2O_4 * t} \quad (3)$$

where *n* substrate is the number of moles of the substrate, C is conversion, *n* $ZnFe_2O_4$ is the number of moles of NP, *D* $ZnFe_2O_4$ is the dispersion and *t* is the time.

3.6. Experimental Procedure for Reusing of the Catalyst

The $ZnFe_2O_4$-NP were recycled and reused with the same reaction conditions. The recycle procedure was as follows:

- Removed the NP from the reaction by using a magnet;
- Washing the NP two times with 1:1 nano water and ethanol;
- Drying the NP in the oven.

4. Conclusions

In this study, we synthesized the phyto-mediated NP of $ZnFe_2O_4$ using *Boswellia carterii* extract. The NP IR spectroscopy, Mössbauer spectroscopy, FESEM and HRTEM studies and magnetic measurements were used. The powder XRD indicated a cubic spinel ferrite with an average diameter of 8 nm as indicated by the FESEM results. The material showed excellent catalytic activity towards valorization of lignin with high activity and selectivity. The oxidation of vanillyl alcohol to vanillin with selectivity up to 99% at a conversion over 98% and turn-over frequency values up to 1600 h^{-1} were obtained in the presence of H_2O_2 and base. The amount and nature of the added base had a significant effect on the reactivity.

Compared to conventional protocols, the advantages of this protocol presented in this study are: (1) high potential catalysis for vanillyl alcohol oxidation, (2) robust production of desired vanillin, (3) green and environmentally friendly conditions and (4) green and sustainable catalyst preparation, (5) unique magnetic nature of the NP of $ZnFe_2O_4$ and (5) catalyst selectivity in the oxidative reaction of lignin substrates models to produce more valuable products.

Author Contributions: Conceptualization, A.A.-H. and D.T.; methodology, A.A.-H.; Q.M.; I.B. and S.M.; software, Q.M. and I.B.; validation, A.A.-H. and S.M.; formal analysis, A.A.-H.; investigation, A.A.-H.; resources, A.A.-H., Q.M.; I.B. and S.M.; data curation, A.A.-H. and T.H.; writing—original draft preparation, A.A.-H. and S.M.; writing—review and editing, A.A.-H.; S.M.; D.T. and T.H.; visualization, A.A.-H.; S.M. and T.H.; supervision, A.A.-H.; project administration, A.A.-H. and T.H; funding acquisition, A.A.-H. All authors have read and agreed to the published version of the manuscript.

Funding: This research was supported by Deanship of Academic Research at the University of Jordan.

Acknowledgments: The Jordanian Cell Therapy Center (CTC) is acknowledged for the SEM imaging. The University of Jordan is acknowledged for granting Sami Mahmood (S.M.) a Sabbatical leave spent at Michigan State University and granting Deeb Taher (D.T.) a Scientific Research Visit spent at Michigan State University. Deeb Taher personally acknowledges The Arab Fund for Economic and Social Development (AFESD) for granting him ZAMALAT Scientific Research Visit to the Michigan State University. This research was part of a close collaboration between the University of Jordan and the Institute for Atmospheric and Earth System Research (INAR / Physics, University of Helsinki) via the Academy of Finland Center of Excellences (project No. 272041 and 1307537).

Conflicts of Interest: The authors declare no conflict of interest.

References

1. Vennestrøm, P.N.R.; Osmundsen, C.M.; Christensen, C.H.; Taarning, E. Beyond petrochemicals: The renewable chemicals industry. *Angew. Chem.* **2011**, *50*, 10502–10509. [CrossRef] [PubMed]
2. Bozell, J.J.; Petersen, G.R. Technology development for the production of biobased products from biorefinery carbohydrates—The US Department of Energy's "Top 10" revisited. *Green Chem.* **2010**, *12*, 539–554. [CrossRef]
3. Zakzeski, J.; Bruijnincx, P.C.A.; Jongerius, A.L.; Weckhuysen, B.M. The Catalytic Valorization of Lignin for the Production of Renewable Chemicals. *Chem. Rev.* **2010**, *110*, 3552–3599. [CrossRef]
4. Giummarella, N.; Zhang, L.; Henriksson, G.; Lawoko, M. Structural features of mildly fractionated lignin carbohydrate complexes (LCC) from spruce. *RSC Adv.* **2016**, *6*, 42120–42131. [CrossRef]
5. Rezanowich, A.; Goring, D. Polyelectrolyte expansion of a lignin sulfonate microgel. *J. Colloid Sci.* **1960**, *15*, 452–471. [CrossRef]
6. Behling, R.; Valange, S.; Chatel, G. Heterogeneous catalytic oxidation for lignin valorization into valuable chemicals: What results? What limitations? What trends? *Green Chem.* **2016**, *18*, 1839–1854. [CrossRef]

7. Perlack, R.D.; Wright, L.L.; Turhollow, A.F.; Graham, R.L.; Stokes, B.J.; Erbach, D.C. *Biomass as Feedstock for A Bioenergy and Bioproducts Industry: The Technical Feasibility of A Billion-Ton Annual Supply*; Oak Ridge National Laboratory: Oak Ridge, TN, USA, 2005.
8. Lange, H.; Decina, S.; Crestini, C. Oxidative upgrade of lignin—Recent routes reviewed. *Eur. Polym. J.* **2013**, *49*, 1151–1173. [CrossRef]
9. Azarpira, A.; Ralph, J.; Lu, F. Catalytic alkaline oxidation of lignin and its model compounds: A pathway to aromatic biochemicals. *BioEnergy Res.* **2014**, *7*, 78–86. [CrossRef]
10. Dai, J.; Patti, A.F.; Saito, K. Recent developments in chemical degradation of lignin: Catalytic oxidation and ionic liquids. *Tetrahedron Lett.* **2016**, *57*, 4945–4951. [CrossRef]
11. Pan, J.; Fu, J.; Lu, X. Microwave-assisted oxidative degradation of lignin model compounds with metal salts. *Energy Fuels* **2015**, *29*, 4503–4509. [CrossRef]
12. Liu, W.J.; Jiang, H.; Yu, H.Q. Thermochemical conversion of lignin to functional materials: A review and future directions. *Green Chem.* **2015**, *17*, 4888–4907. [CrossRef]
13. Huber, G.W.; Iborra, S.; Corma, A. Synthesis of transportation fuels from biomass: Chemistry, catalysts, and engineering. *Chem. Rev.* **2006**, *106*, 4044–4098. [CrossRef] [PubMed]
14. Chen, W.H.; Tu, Y.J.; Sheen, H.K. Disruption of sugarcane bagasse lignocellulosic structure by means of dilute sulfuric acid pretreatment with microwave-assisted heating. *Appl. Energy* **2011**, *88*, 2726–2734. [CrossRef]
15. Stahl, S.S.; Coon, J.; Rahimi, A.; Ulbrich, A. Selective CeO Bond Cleavage of Oxidized Lignin and Lignin-Type Materials into Simple Aromatic Compounds. U.S. Patent 9359391, 7 June 2016.
16. Tolba, R.; Tian, M.; Wen, J.; Jiang, Z.-H.; Chen, A. Electrochemical oxidation of lignin at IrO_2-based oxide electrodes. *J. Electroanal. Chem.* **2010**, *649*, 9–15. [CrossRef]
17. Gharehkhani, S.; Zhang, Y.; Fatehi, P. Lignin-derived platform molecules through TEMPO catalytic oxidation strategies. *Prog. Energy Combust. Sci.* **2019**, *72*, 59–89. [CrossRef]
18. Jha, A.; Patil, K.R.; Rode, C.V. Mixed Co–Mn oxide-catalysed selective aerobic oxidation of vanillyl alcohol to vanillin in base free conditions. *ChemPlusChem* **2014**, *78*, 1384–1392. [CrossRef]
19. Védrine, J.C. Heterogeneous catalysis on metal oxides. *Catalysis* **2017**, *7*, 341. [CrossRef]
20. Khan, I.; Saeed, K.; Khan, I. Nanoparticles: Properties, applications and toxicities. *Arab. J. Chem.* **2019**, *12*, 908–931. [CrossRef]
21. Jeevanandam, J.; Barhoum, A.; Chan, Y.S.; Dufresne, A.; Danquah, M.K. Review on nanoparticles and nanostructured materials: History, sources, toxicity and regulations. *Beilstein J. Nanotechnol.* **2018**, *9*, 1050–1074. [CrossRef]
22. Holišová, V.; Urban, M.; Kolenˇcík, M.; Nˇemcová, Y.; Schröfel, A.; Peikertová, P.; Slabotinský, J.; Kratošová, G. Biosilica-nanogold composite: Easy-to-prepare catalyst for soman degradation. *Arab. J. Chem.* **2019**, *12*, 262–271. [CrossRef]
23. Sharma, N.; Ojha, H.; Bharadwaj, A.; Pathak, D.P.; Sharma, R.K. Preparation and catalytic applications of nanomaterials: A review. *RSC Adv.* **2015**, *5*, 53381–53403. [CrossRef]
24. Ye, Z.; Giraudon, J.M.; Nuns, N.; Simon, P.; De Geyter, N.; Morent, R.; Lamonier, J.F. Influence of the preparation method on the activity of copper-manganese oxides for toluene total oxidation. *Appl. Catal. B* **2018**, *223*, 154–166. [CrossRef]
25. Muñoz-Batista, M.J.; Bertolini, G.R.; Cabello, C.I.; Luque, R.; Rodríguez-Castellón, E.; Kubacka, A.; Fernández-García, M. Novel (NH4) 4 $[NiMo_6O_{24}H_6]$ $5H_2O$–TiO_2 composite system: Photo-oxidation of toluene under UV and sunlight-type illumination. *Appl. Catal. B* **2018**, *238*, 381–392. [CrossRef]
26. Reda, S.M. Synthesis and optical properties of CdS quantum dots embedded in silica matrix thin films and their applications as luminescent solar concentrators. *Acta Mater.* **2008**, *56*, 259–264. [CrossRef]
27. Zhang, J.; Langille, M.R.; Mirkin, C.A. Synthesis of silver nanorods by low energy excitation of spherical plasmonic seeds. *Nano Lett.* **2011**, *11*, 2495–2498. [CrossRef] [PubMed]
28. Nasrabadi, H.T.; Abbasi, E.; Davaran, S.; Kouhi, M.; Akbarzadeh, A. Bimetallic nanoparticles: Preparation, properties, and biomedical applications. *Artif. Cells Nanomed. Biotechnol.* **2016**, *44*, 376–380. [CrossRef] [PubMed]
29. Zhang, B.P.; Zhang, J.L.; Chen, F. Preparation and Characterization of Magnetic TiO_2/$ZnFe_2O_4$ Photocatalysts by a sol-gel Method. *Res. Chem. Intermed.* **2008**, *34*, 375–380. [CrossRef]

30. Fierascu, R.C.; Fierascu, I.; Lungulescu, E.M.; Nicula, N.; Somoghi, R.; Di¸tu, L.M.; Ungureanu, C.; Sutan, A.N.; Drăghiceanu, O.A.; Paunescu, A. Phytosynthesis and radiation-assisted methods for obtaining metal nanoparticles. *J. Mater. Sci.* **2019**, *55*, 1915–1932. [CrossRef]
31. Laokul, P.; Amornkitbamrung, V.; Seraphin, S.; Maensiri, S. Characterization and Magnetic Properties of Nanocrystalline $CuFe_2O_4$, $NiFe_2O_4$, $ZnFe_2O_4$ Powders Prepared by the Aloe Vera Extract Solution. *Curr. Appl. Phys.* **2011**, *11*, 101–108. [CrossRef]
32. Elavazhagan, T.; Arunachalam, K.D. Memecylon edule leaf extract mediated green synthesis of silver and gold nanoparticles. *Int. J. Nanomed.* **2011**, *6*, 1265–1278. [CrossRef]
33. Iravani, S. Green synthesis of metal nanoparticles using plants. *Green Chem.* **2011**, *13*, 2638–2650. [CrossRef]
34. Kavitha, K.S.; Baker, S.; Rakshith, D.; Kavitha, H.U.; Rao, H.C.Y.; Harini, B.P.; Satish, S. Plants as green source towards synthesis of nanoparticles. *Int. Res. J. Biol. Sci.* **2013**, *2*, 66–76.
35. Zhou, Z.H.; Xue, J.M.; Chan, H.S.O.; Wang, J. Nanocomposites of $ZnFe_2O_4$ in silica: Synthesis, magnetic and optical properties. *Mater. Chem. Phys.* **2002**, *75*, 181–185. [CrossRef]
36. Valenzuela, M.A.; Bosch, P.; Jimenez-Becerrill, J.; Quiroz, O.; Paez, A.I. Preparation, characterization and photocatalytic activity of ZnO, Fe_2O_3 and $ZnFe_2O_4$. *J. Photochem. Photobiol. A* **2002**, *148*, 177–182. [CrossRef]
37. Brusotti, G.; Cesari, I.; Dentamaro, A.; Caccialanza, G.; Massolini, G. Isolation and characterization of bioactive compounds from plant resources: The role of analysis in the ethnopharmacological approach. *J. Pharm. Biomed. Anal.* **2014**, *87*, 218–228. [CrossRef]
38. Smit, J.; Wijn, H.P.J. *Ferrites*; Wiley: New York, NY, USA, 1959.
39. Mahmood, S.H. Properties and Synthesis of Hexaferrites. In *Hexaferrite Permanent Magnetic Materials*; Mahmood, S.H., Abu-Aljarayesh, I., Eds.; Materials Research Forum LLC: Millersville, PA, USA, 2016; pp. 74–110.
40. Singh, J.P.; Srivastava, R.C.; Agrawal, H.M.; Kushwaha, R.P.S. ^{57}Fe Mössbauer spectroscopic study of nanostructured zinc ferrite. *Hyperfine Interact.* **2008**, *183*, 221–228. [CrossRef]
41. Mahmood, S.H. Magnetic anisotropy in fine magnetic particles. *J. Magn. Magn. Mater.* **1993**, *118*, 359–364. [CrossRef]
42. Lehlooh, A.F.; Mahmood, S.; Abu-Aljarayesh, I. Mössbauer and X-ray diffraction studies of heat-treated Fe_3O_4 fine particles. *J. Magn. Magn. Mater.* **1994**, *136*, 143–148. [CrossRef]
43. Mahmood, S.H.; Abu-Aljarayesh, I. On the static and time-dependent magnetic properties of Fe_3O_4 fine particles: Effect of oxidation. *J. Magn. Magn. Mater.* **1993**, *118*, 193–199. [CrossRef]
44. Lin, Q.; Xu, J.; Yang, F.; Lin, J.; Yang, H.; He, Y. Magnetic and Mössbauer spectroscopy studies of zinc-substituted cobalt ferrites prepared by the sol-gel method. *Materials* **2018**, *11*, 1799. [CrossRef]
45. Mate, V.R.; Jha, A.; Joshi, U.D.; Patil, K.R.; Shirai, M.; Rode, C.V. Effect of preparation parameters on characterization and activity of Co_3O_4 catalyst in liquid phase oxidation of lignin model substrates. *Appl. Catal. A* **2014**, *487*, 130–138. [CrossRef]
46. Tarasov, A.L.; Kustov, L.M.; Bogolyubov, A.A.; Kiselyov, A.S.; Semenov, V.V. New and efficient procedure for the oxidation of dioxybenzylic alcohols into aldehydes with Pt and Pd-based catalysts under flow reactor conditions. *Appl. Catal. A* **2009**, *366*, 227–231. [CrossRef]
47. Shilpy, M.; Ehsan, M.A.; Ali, T.H.; Abd Hamid, S.B.; Ali, E. Performance of cobalt titanate towards H_2O_2 based catalytic oxidation of lignin model compound. *RSC Adv.* **2015**, *5*, 79644–79653. [CrossRef]
48. Zope, B.N.; Hibbitts, D.D.; Neurock, M.; Davis, R.J. Reactivity of the gold/water interface during selective oxidation catalysis. *Science* **2010**, *330*, 74–78. [CrossRef]
49. Tsunoyama, H.; Sakurai, H.; Negishi, Y.; Tsukuda, T. Size specific catalytic activity of polymer-stabilized gold nanoclusters for aerobic alcohol oxidation in water. *J. Am. Chem. Soc.* **2005**, *127*, 9374–9375. [CrossRef]
50. Tsunoyama, H.; Tsukuda, T.; Sakurai, H. Synthetic application of PVP-stabilized Au nanocluster catalyst to aerobic oxidation of alcohols in aqueous solution under ambient conditions. *Chem. Lett.* **2007**, *36*, 212–221. [CrossRef]
51. Higashimoto, S.; Kitao, N.; Yoshida, N.; Sakura, T.; Azuma, M.; Ohue, H.; Sakata, Y. Selective photocatalytic oxidation of benzyl alcohol and its derivatives into corresponding aldehydes by molecular oxygen on titanium dioxide under visible light irradiation. *J. Catal.* **2009**, *266*, 279–285. [CrossRef]
52. Higashimoto, S.; Suetsugu, N.; Azuma, M.; Ohue, H.; Sakata, Y. Efficient and selective oxidation of benzylic alcohol by O_2 into corresponding aldehydes on a TiO_2 photocatalyst under visible light irradiation: Effect of phenyl-ring substitution on the photocatalytic activity. *J. Catal.* **2010**, *274*, 76–83. [CrossRef]

53. Higashimoto, S.; Okada, K.; Morisugi, T.; Azuma, M.; Ohue, H.; Kim, T.H.; Matsuoka, M.; Anpo, M. Effect of Surface Treatment on the Selective Photocatalytic Oxidation of Benzyl Alcohol into Benzaldehyde by O_2 on TiO_2 Under Visible Light. *Top. Catal.* **2010**, *53*, 578–583. [CrossRef]
54. Kim, S.; Choi, W. Visible-Light-Induced Photocatalytic Degradation of 4-Chlorophenol and Phenolic Compounds in Aqueous Suspension of Pure Titania: Demonstrating the Existence of a Surface-Complex-Mediated Path. *J. Phys. Chem. B* **2005**, *109*, 5143–5144. [CrossRef]
55. Li, C.-J.; Xu, G.-R.; Zhang, B.; Gong, J.R. High selectivity in visible-light-driven partial photocatalytic oxidation of benzyl alcohol into benzaldehyde over single-crystalline rutile TiO_2 nanorods. *Appl. Catal. B* **2012**, *201*, 115–116. [CrossRef]
56. Samiolo, L.; Valigi, M.; Gazzoli, D.; Amadelli, R. Visible-light photocatalysis in nitrogen-doped titanium oxides. *Electrochim. Acta* **2010**, *55*, 7788–7795. [CrossRef]
57. Fargues, C.; Mathias, A.; Rodrigues, A. Kinetics of vanillin production from kraft lignin oxidation. *Ind. Eng. Chem. Res.* **1996**, *35*, 28–36. [CrossRef]
58. Gladysz, J.A. The Experimental Assay of Catalyst Recovery: General Concepts. In *Recoverable and Recyclable Catalysts*; Benaglia, M., Ed.; Wiley: Chichester, UK, 2009; Chapter 1, pp. 1–14.
59. Luadthong, C.; Khemthong, P.; Nualpaeng, W.; Faungnawakij, K. Copper ferrite spinel oxide catalysts for palm oil methanolysis. *Appl. Catal. A Gen.* **2016**, *525*, 68–75. [CrossRef]
60. Zheng, M.; Lin, K.A.; Lin, C. TEMPO-Functionalized Silica as an Efficient and Recyclable Oxidation Catalyst for Conversion of a Lignin Model Compound to Value-Added Products. *Waste Biomass Valoriz.* **2019**, 1–12. [CrossRef]
61. Ramana, S.; Rao, B.G.; Venkataswamy, P.; Rangaswamy, A.; Reddy, B.M. Nanostructured Mn-doped ceria solid solutions for efficient oxidation of vanillyl alcohol. *J. Mol. Catal. A* **2016**, *415*, 113–121. [CrossRef]